Desalination and Water Treatment
www.deswater.com

doi: 10.5004/dwt.2023.29274

285 (2023) 264–273
February

Effective removal of methylene blue from aqueous solution by adsorption onto gasification char: isotherm, kinetic and thermodynamics studies

Nurul Najihah Ahmad[a], Anis Atikah Ahmad[a,b,*], Azduwin Khasri[a,b]

[a]*Faculty of Chemical and Engineering Technology, Universiti Malaysia Perlis, Kompleks Pusat Pengajian Jejawi 3, 02600 Arau, Perlis, Malaysia, emails: anisatikah@unimap.edu.my (A.A. Ahmad), s171141204@studentmail.unimap.edu (N.N. Ahmad), azduwin@unimap.edu.my (A. Khasri)*
[b]*Centre of Excellence, Water Research and Environmental Sustainability Growth (WAREG), Universiti Malaysia Perlis, 02600 Arau, Perlis, Malaysia*

Received 20 October 2022; Accepted 22 December 2022

ABSTRACT

This study presents the preparation of oil palm empty fruit bunch (OPEFB) activated char from gasification plant residues via phosphoric acid chemical treatment for adsorption of methylene blue (MB) in aqueous solution. The Fourier-transform infrared (FTIR), scanning electron microscopy (SEM) and Brunauer–Emmett–Teller (BET) analysis were conducted to identify the characteristic of OPEFB. Adsorption experiments were carried out to determine the effects of initial dye concentration 100–300 mg/L, contact time, pH 2–10 and temperature 30°C–60°C. The optimum conditions were achieved at adsorbent dosage, pH, initial dye concentration and temperature of 0.2 g/200 mL, 6, 100 mg/L and 60°C, respectively with 91.44% of MB removal. From isotherm study, the Freundlich isotherm model fitted the adsorption data very well owing to its higher value of correlation factor (R^2 = 0.9352), compared to Langmuir model (R^2 = 0.8682). The Langmuir maximum monolayer capacity, q_m was estimated at 167.2 mg/g. The results from the kinetic study showed that the MB adsorption followed a pseudo-second-order kinetic model (R^2 = 0.9216–0.9581). The adsorption of the MB dye onto OPEFB activated char was an endothermic and spontaneous process with $\Delta H°$, $\Delta G°$ and $\Delta S°$ values of 58.379 kJ/mol, –0.70505 kJ/mol and 194.955 J/mol·K, respectively. The obtained results suggest that the OPEFB char could be a promising candidate as an adsorbent for MB removal.

Keywords: Gasification char; Oil palm empty fruit bunch; Adsorption; Methylene blue; Chemical activation; Activated carbon

1. Introduction

The release of substantial amount of pollutants into the environment due to the rapid growth in industrial and agricultural activities is one of the key challenges worldwide. Dyes are type of pollutant that must be sequestered from wastewater before being released into the aquatic environment due to the toxicity and negative effects on aquatic life. The most widely used dye in the textile industry is methylene blue (MB), which is applied in dyeing cotton, coloring paper, leather, silk and wools [1]. The presence of MB in water stream can damage the balance of the environmental ecosystem characterized by the contamination and death of aquatic organisms [2]. Besides, their degradation products may be mutagenic and carcinogenic and may cause allergic dermatitis, dysfunction of kidney, skin irritation, brain, liver, reproductive and central nervous system problems [3]. Therefore, it is vital to strictly manage the discharge of this pollutant into the water stream due to its harmful hazard and negative environmental impacts [4].

Many researchers are currently using various methods to treat dye wastewater. Physical, chemical and biological treatment methods commonly used include: flocculation,

* Corresponding author.

membrane filtration, advanced oxidation ozonation, adsorption and biodegradation [5]. The most efficient method used for quick removal of dyes from the aqueous solution is the adsorption. Adsorption is widely employed owing to its benefits such as low cost, high efficiency, reusability, simplicity, flexibility, easy operation, and insensitivity to hazardous chemicals compared to other treatment techniques [6–8]. Adsorption is a physical–chemical treatment of wastewater where the dissolved molecule is attached to an adsorbent surface by means of physical and chemical properties [9]. Meanwhile, the biological treatment method is commonly operated via numerous microorganisms to decolorize dye molecules under aerobic or anaerobic environment and is feasible to lower the concentration of contaminants. In addition, it was reported that this method is insufficient in decolorization owing to the complicated structures and difficult biodegradation of dyestuff as well as less predictability and requires considerable time and space [10]. The adsorbents like activated carbon (AC) are foremost promising material for adsorption of MB owing to its high adsorption efficiency, supported on its large surface area, micro-porosity structure and high surface reactivity. However, the appliance of AC in water purification is usually limited by the high cost of this material, which is an obstacle especially for industries in developing countries [11].

Gasification char is the finer component of the gasifier solid residuals that comprised of unreacted carbon with several amounts of siliceous ash and it possesses good characteristic as an adsorbent due to its well-developed pore properties [12]. Gasification is a thermochemical process, produces syngas or producer gas for power or combined heat and power applications in the presence of gasifying agents like steam, air and carbon dioxide also yields a char by-product [13]. Mohan et al. [14] reported that the gasification char accounts for only about 10% of the products as the quantity becomes appreciable at an industrial-scale where feedstock is in tonnes. Feedstock for gasification has been sourced from biomass [15–17], coal [18–20] and municipal solid wastes [21–23]. The agricultural solid waste, industrial solid waste, agricultural by-products and biomass are utilised as low-cost adsorbents in wastewater treatment [5]. Sharma et al. [24] reported that various agricultural by-products like olive stones, peach stones, pistachio nut shells, date pits, sea sand, eggshells, banana peel, pumpkin and rice husk were within the production of low-cost adsorbents. However, there are limited number of studies on the utilization of char residues from biomass gasification plant. The literature regarding its application in adsorption is somewhat limited to heavy metals and tar removal. Only few researchers reported that the dye adsorptions utilizing gasification char residues (GCR) as adsorbent or precursor for AC. For instance, Maneerung et al. [25] investigated the removal of Rhodamine-B (RhB) using AC from gasification of mesquite wood chips in downdraft fixed-bed gasifier. They reported that the prepared AC exhibited high RhB adsorption capability. This was owing to its high specific surface area (776.5 m^2/g) and the abundance of carboxyl and hydroxyl groups. They also discovered that the experimental data well fitted Langmuir model with the maximum monolayer adsorption capability of 189.8 mg/g. They concluded that the utilization of GCR as a precursor of AC lowers the AC production cost; offers a cost effective and environmental-friendly measures in recycling char; and lessening the environmental problems related to its disposal.

Malaysia is one of the world's amongst oil palm producers, producing 47% of the world's supply of palm oil [26]. Approximately, 127 million tons of oil palm wastes are generated from the oil palm industry annually in Malaysia which consists of 64.19, 26.08, 15.99, 14.87, and 6.49 million tons of palm frond (PF), empty fruit bunch (EFB), mesocarp fiber (MF), palm trunk (PT), and palm kernel shell (PKS) [27]. Owing to the abundance of oil palm empty fruit bunch (OPEFB) as well as its high carbon content (42–50 wt.%), it has a potential to be a pre-cursor for AC production in wastewater treatment application. Thus, this study aimed to investigate the OPEFB char performance in MB removal by adsorption. Besides, its functional groups, surface morphology and specific surface area will be analyzed and the isotherm, kinetic and thermodynamic studies will be performed to determine the governing mechanism for MB adsorption.

2. Materials and methods

2.1. Materials

The required materials in the study were char from OPEFB which was collected from a local commercial gasification plant, MB (HmbG Chemicals, Malaysia), phosphoric acid (H_3PO_4) (Bendosen, Malaysia), 0.1 M sodium hydroxide (NaOH) (HmbG Chemicals, Malaysia) and 0.1 M hydrochloric acid (HCl) (QReC, Malaysia).

2.2. Sample preparation

OPEFB chars were collected from a commercial gasification plant in Selangor, Malaysia. The sample was washed to remove dirt particles from its surface and dried in an oven at 105°C for 24 h to ensure that the moisture content was reduced. The dried sample was sieved to discrete sizes (500 μm). Then, the sample of OPEFB char was soaked in phosphoric acid solution with an impregnation (char:H_3PO_4) ratio of 1:1 (wt./vol.). The impregnated char was kept at room temperature for 1 h and mixed vigorously for 30 min. Finally, the sample was then rinsed with deionized water until the sample reaches pH 6–7 and dried at 110°C for 24 h [28].

2.3. Characterization of OPEFB

Fourier-transform infrared (FTIR) spectrometer (Perkin Elmer, USA) analysis was performed to investigate the functional groups existed in untreated OPEFB and treated OPEFB char. The scanning electron microscope (SEM) and Brunauer–Emmett–Teller (BET) analysis were conducted to reveal the surface morphology and pore properties of OPEFB before and after the chemical activation process [29].

2.4. Adsorption experiment

2.4.1. Effect of initial concentration and contact time on MB adsorption

Adsorption experiment was tested in a set of 250 mL Erlenmeyer flasks containing 0.20 g adsorbent and 200 mL

dye solutions with the different initial concentrations of 100, 150, 200, 250 and 300 mg/L [30]. The flasks were agitated in the shaker at 150 rpm and at temperature, 30°C for 4 h of contact time until equilibrium was reached [31]. The mixture was filtered, and the concentration of the filtrate was measured by UV-Vis spectrophotometer. MB uptake at equilibrium, q_e (mg/g), was calculated using Eq. (1).

$$q_e = \frac{\left(C_0 - C_e\right)V}{W} \tag{1}$$

where C_0 is liquid-phase concentrations of dye at initial (mg/L), C_e is equilibrium dye concentration (mg/L), V is volume of the solution (L) and W is mass of adsorbent used (g). The removal percentage of MB was estimated using Eq. (2).

$$R(\%) = \frac{C_0 - C_t}{C_0} \times 100\% \tag{2}$$

where C_0 is initial concentration of MB (mg/L), C_t is t-time concentration of MB (mg/L) and R is removal percentage (%) of MB.

2.4.2. Effect of solution pH on MB adsorption capacity

Effect of pH on MB removal was measured by different pH solution starting from 2 to 10 with initial MB concentration of 100 mg/L, OPEFB char dosage of 0.20 g/200 mL and adsorption temperature at 30°C for 24 h [32]. The effect of solution pH was tested in the range of 2–10 and measured using pH meter. 0.1 M NaOH and 0.1 M HCl were used to adjust the solution pH.

2.4.3. Effect of temperature on MB adsorption capacity

The effect of temperature on the adsorption capacity of OPEFB char was examined at 30°C, 45°C and 60°C with initial MB concentration of 100 mg/L, OPEFB char dosage of 0.20 g/200 mL for 24 h.

2.5. Thermodynamic study

The thermodynamics parameters of MB adsorption were studied by applying the Van't Hoff Eq. (3) as follows:

$$\ln K_c = \frac{\Delta S^\circ}{R} - \frac{\Delta H^\circ}{RT} \tag{3}$$

where k_c is the equilibrium constant, ΔG° (kJ/mol) is the Gibb's energy change, ΔH° (kJ/mol) is the enthalpy change, ΔS° (kJ/mol·K) is the entropy change and R is the universal gas constant. The R value is 8.314 J/mol·K. The standard free energy change was calculated by Eqs. (4) and (5):

$$K_c = \frac{Q_e}{C_e} \tag{4}$$

$$\Delta G^\circ = -RT \ln K_c \tag{5}$$

2.6. Isotherm and kinetic adsorption using non-linear models

The experimental results were fitted to isotherm and kinetic adsorption models using non-linear models by employing MATLAB curve fitting tool. The equilibrium adsorption data was fitted to Langmuir and Freundlich isotherm models while the kinetic data was fitted to pseudo-first-order and pseudo-second-order kinetic models. Both non-linear models were compared based on the best fitted correlation factor, R^2.

2.6.1. Langmuir isotherm model

The Langmuir isotherm model is given by Eq. (6):

$$q_e = \frac{q_{\max} K_L C_e}{1 + K_L C_e} \tag{6}$$

where $q_{\max}$ is maximum adsorption capacity (mg/g), K_L is Langmuir constant (L/mg), C_e is adsorbate (dye) concentration at equilibrium (mg/L) and q_e is quantity of MB dye adsorbed per gram adsorbent (mg/g).

2.6.2. Freundlich isotherm model

The non-linear model of Freundlich is given in Eq. (7):

$$q_e = K_F C_e^{1/n} \tag{7}$$

where K_F is adsorbent adsorption capacity (mg/g·(L/mg)$^{1/n}$) and n is adsorbent adsorption intensity.

2.6.3. Pseudo-first-order model

The non-linear form of pseudo-first-order model is given in Eq. (8) [28]:

$$q_t = q_e\left(1 - e^{k_1 t}\right) \tag{8}$$

2.6.4. Pseudo-second-order model

The pseudo-second-order model is given in Eq. (9):

$$q_t = \frac{k_2 q_e^2 t}{1 + k_2 q_e t} \tag{9}$$

where k_2 is the rate constant of pseudo-second-order (g/mg·min).

3. Results and discussion

3.1. Sample functional groups

The FTIR spectra for the untreated OPEFB char and the treated OPEFB char are shown in Fig. 1. The untreated OPEFB char demonstrated an absorption band at 3,049.2 cm^{-1}, which was attributed to O–H stretching mode of hydroxyl functional group. The adsorbed moisture content in the untreated OPEFB char led the O–H

group [33]. The bands at 1,427.7 and 1,371 cm^{-1} appeared on untreated OPEFB char and treated OPEFB char refers to the O–H bending mode of hydroxyl groups. An absorption band at 3,638 and 3,038.6 cm^{-1} was detected in treated OPEFB char and this band was also assigned to O–H hydroxyl group. Its intensity were greatly increased due to the vaporization of moisture content through activation process and adsorption of water from atmosphere onto the surface of AC. The absorption band located at 1,582 cm^{-1} was detected for untreated OPEFB char, which shows the presence of C=C vibration in aromatic rings. An absorption band at 1,566.2 cm^{-1} was detected in treated OPEFB char and this band also was assigned to C=C vibration in aromatic rings. The characteristic peaks at 1,723.6 cm^{-1} corresponds to the stretching of C=O bonds. The absence of absorption band at 1,723.6 cm^{-1} for treated OPEFB char sample showed that carbonyl group was greatly reduced after acid pre-treatment and activation [34].

The spectra of all the samples displayed the bands containing O–H, C=C and C=O groups at varied absorption wavenumbers that give rise to efficient reduction of pollutants in targeted wastewaters. The changes discovered in the FTIR spectra confirmed that these functional groups were identified on the surface of the OPEFB char before and after acid pre-treatment. This result showed that the hydroxyl (–OH) groups enriched the surface of the OPEFB char prepared from chemical activation, which can significantly enhance the adsorption performance as reported by Maneerung et al. [25].

3.2. Sample morphology

The SEM was used to identify the surface morphological characteristics of the samples for further comparison of porosity. The SEM images of the untreated OPEFB char and the treated OPEFB char are shown in Fig. 2a and b, which clearly show the differences. In Fig. 2a, the untreated OPEFB char had very little pores available on the surface and had a thick wall structure compared to the acid treated OPEFB char as shown in Fig. 2b. Besides, the small cell

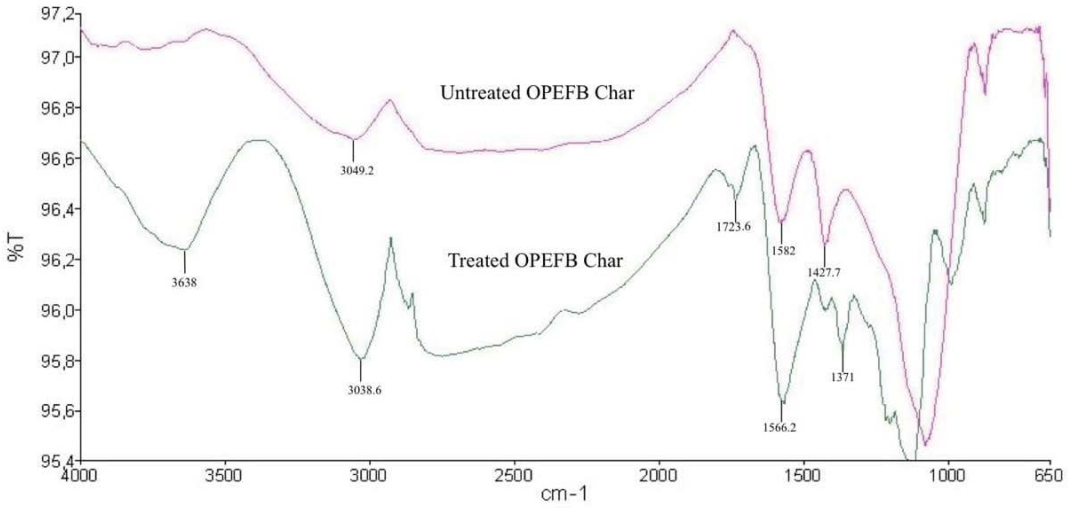

Fig. 1. FTIR spectrum for untreated OPEFB char and treated OPEFB char.

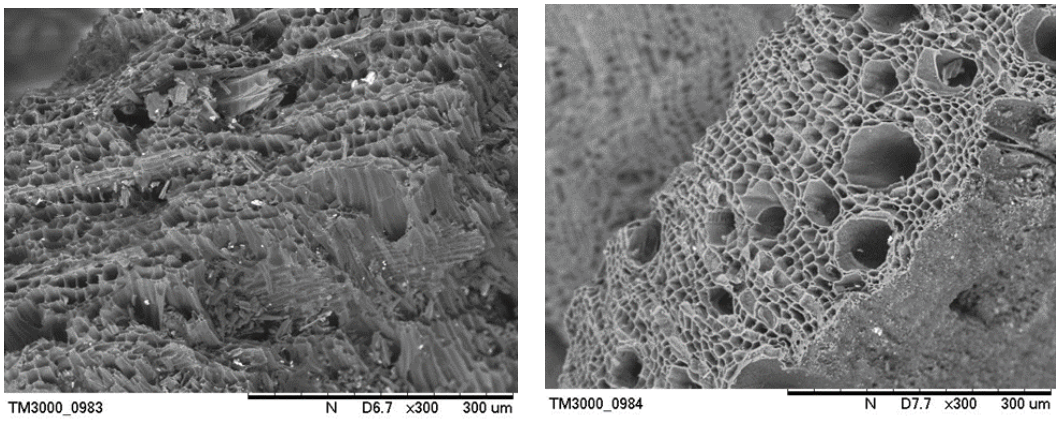

(a) (b)

Fig. 2. SEM images of (a) untreated OPEFB char (×300) and (b) treated OPEFB char (×300).

cavity with non-developed porosity and patches of crack are observed in Fig. 2a, as well as the cell wall breakdown [35]. After the activation process, a well-developed porous structure with quite uniform pore was formed as indicated in Fig. 2b. This indicates that the porosity was expanded due to activation agent and process [36–38]. In pre-treatment, the removal of an excessive activating agent and by-products resulting from the activation process during the washing step leads to a material with a well-developed surface and a porous structure. The results showed that the activation of OPEFB char with phosphoric acid (H_3PO_4) and heat treatment successfully produced pores, which is expected to be beneficial to the adsorption of pollutants. Like other chemical activators, H_3PO_4 plays an important role as a dehydrating agent, which can penetrate deeply into the carbon structure, leading to the formation of pores on the surface of the AC precursor [39]. These results also indicate that there was a development of pore structure of the treated OPEFB char during the activation process, which may involve three stages: opening the unreachable pores, creating the new pores, and enlarging the existing pores.

3.3. Specific surface area analysis

Table 1 shows surface area, total pore volume (TPV) and average pore diameter (APD) of untreated OPEFB and treated OPEFB chars. The untreated OPEFB char possessed a relatively low BET surface area and a TPV of 258.87 m^2/g and 0.1558 cm^3/g, respectively. After the chemical impregnation step, the surface area and TPV increased as a result of pore widening and development which can be seen in Fig. 2.

3.4. Adsorption performance

3.4.1. Effect of initial MB dye concentration and contact time

Fig. 3 shows the percentage removal of MB dye vs. the time (h) at different initial MB dye concentrations at 30°C with adsorbent dosage of 0.2 g as its constant factor. The initial dye concentration has a pronounced effect on its removal from aqueous solutions. In the present study, the percentage removal of MB increased from 65.65% to 99.77% with decreasing initial concentration of MB from 300 to 100 mg/L. Lower concentration results in a higher percentage of dye removal since there is less MB to be adsorbed at lower concentration compared to higher concentration. At an initial dye concentration of 100 ppm and a contact time of 24 h, the highest percentage removal was almost constant, which was in the range of 99.72%–99.77%. It was found from the study that as the dye concentration and contact time increases, the percentage removal of MB also increases [40]. This is due to the fact that in the process of dye adsorption, before the MB molecules diffuse into the porous structure of the adsorbent, the molecules have to cross the boundary layer film onto the adsorbent surface [41]. Thus, the higher concentration of MB solutions takes relatively longer to adsorb due to the higher number of molecules [42–44].

Table 1
Pore properties of untreated OPEFB and treated OPEFB

	S_{BET} (m^2/g)	TPV (cm^3/g)	APD (nm)
Untreated OPEFB	258.87	0.1558	3.5612
Treated OPEFB	345.43	0.2065	3.4813

3.4.2. Effect of pH

Fig. 4 illustrates the effect of pH on percentage removal of MB on treated OPEFB char by varying the pH of the solution from 2 to 10, with initial MB concentration of 100 mg/L, adsorbent dosage of 0.2 g at 30°C and 24 h of contact time. The same condition was reported by Almoneef et al. [45] as the best adsorption condition for this parameter. The pH of MB solution is one of the most important factors in the adsorption of cationic dye because of its impact on both the surface binding sites of the adsorbent and the ionization process of the dye molecules [46]. It is shown in Fig. 4 that the percentage removal of MB onto treated OPEFB char increased with the increase of pH from 2 to 6 (increased from 11.53% to 82.55%). The reason for this is mainly related to the abundance of OH^- ions at higher pH, which facilitated the electrostatic attractions between the positively charged dye cations and negatively charged adsorption site, thereby increasing the dye uptake. At pH > pH_{pzc} (pH 5.5), the surface charge of OPEFB is mainly negative, which tends to attract the positively charged MB dye since the number of the positively charged groups at

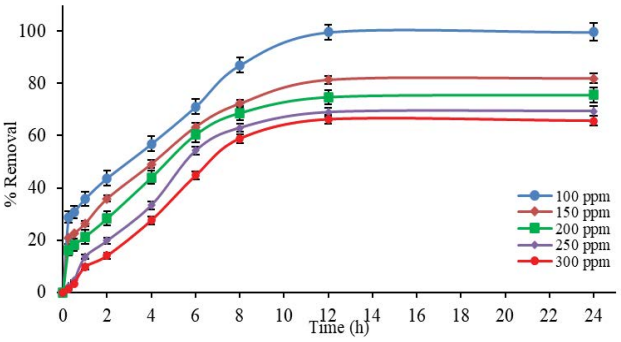

Fig. 3. Effect of initial concentration on percentage removal of MB dye onto treated OPEFB char.

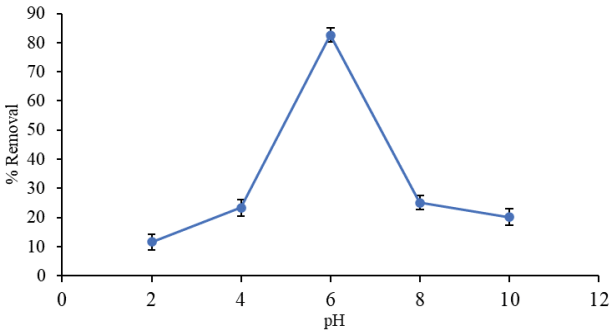

Fig. 4. Effect of pH on percentage removal of MB onto treated OPEFB char.

the OPEFB char surface decreased, while the number of negatively charged groups increased. Hence, the adsorption of MB onto the surface of the OPEFB char increased as the pH increased from 4 to 6. The optimum pH was attained at pH 6. However, a further increase in pH to 10 slightly reduced the percentage removal due to the demethylation of MB in alkaline solution [47]. As the pH of the solution increased, the amount of dye adsorbed decreased considerably. Yu and Luo [48] stated that the pH value of MB solution may affect the surface charge of adsorbent and the functional groups of adsorbates. The same behaviour was observed by many authors including Intarachandra et al. [29], Sajab et al. [49] and Soleimani et al. [50].

3.4.3. Effect of temperature

The effect of temperature on percentage removal of MB onto treated OPEFB char was studied at three different temperature values of 30°C, 45°C and 60°C with the initial MB concentration of 100 mg/L and adsorbent dosage of 0.2 g at pH 6 as the results are presented in Fig. 5. The experimental results showed that the removal of MB increased from 56.95% to 91.44% with increasing temperature from 30°C to 60°C. The higher the temperature, the higher the adsorption ability of MB onto treated OPEFB char [5]. This indicated that the adsorption of MB was a spontaneous endothermic process. The thermal motion, solubility and chemical potential of dye molecules increased as temperature increased. Furthermore, the pore structure of treated OPEFB char was closely related to temperature. The pore structure and number of active adsorption sites of treated OPEFB char increased with the increase of temperature due to thermal expansion. These reasons led to the increase of percentage removal of MB on treated OPEFB char with the increase of temperature as similar findings were reported by Mouni et al. [51] who studied the effect of temperature on MB adsorption at temperature between 25°C–50°C temperature range using kaolin.

3.5. Adsorption thermodynamic

Thermodynamic parameters, including Gibb's free energy change ($\Delta G°$), enthalpy change ($\Delta H°$) and entropy change ($\Delta S°$), serve to evaluate the effect of temperature on the adsorption of MB onto treated OPEFB char. The values of $\Delta H°$ and $\Delta S°$ were then calculated from the slope and intercept of the linear regression of $\ln(k_c)$ vs. $1/T$ for MB initial concentration of 100 mg/L at pH 6 as presented in Fig. 6.

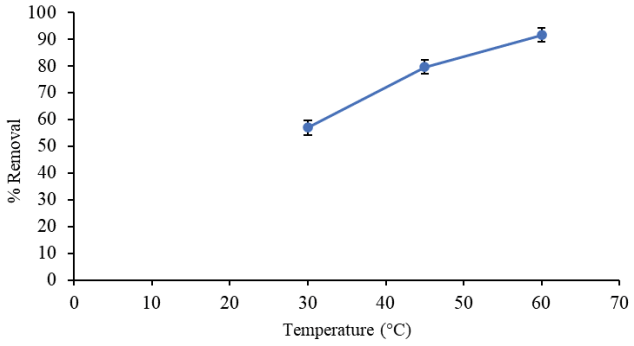

Fig. 5. Effect of temperature on percentage removal of MB onto treated OPEFB char.

Table 2 shows the calculated values for $\Delta H°$, $\Delta S°$, and $\Delta G°$. The positive value of $\Delta H°$ at various temperatures shows that the adsorption process was endothermic. The adsorption process for endothermic processes might be due to a reduction in the viscosity of the solution, which enhanced the rate of diffusion of the adsorbate molecules over the exterior boundary layer and in the interior pores of the adsorbent particles [6,52]. The positive value of $\Delta S°$ showed the affinity of the treated OPEFB char for MB and the increasing randomness at the solid-solution interface during the adsorption process. The $\Delta G°$ values for MB adsorption onto treated OPEFB char were found to be –0.70505 (30°C) kJ/mol, –3.5925 (45°C) kJ/mol and –6.5562 (60°C) kJ/mol. The negative value of $\Delta G°$ indicated the feasibility of the process and the spontaneous nature of the adsorption with a high preference of MB on treated OPEFB char. These result clearly showed that the adsorption process was more favourable at high temperature (60°C) due to the endothermic nature of the adsorption system. Similar trend was reported by Wang et al. [53] and Araújo et al. [54].

3.6. Equilibrium studies

3.6.1. Adsorption isotherms

Fig. 7 illustrates the plots of the Langmuir and Freundlich isotherm models, while Table 3 shows the values of each model parameter. These experimental data fitting isotherms were used in this study to determine the interaction between the amount of dye adsorbed and its equilibrium concentration in solution [55]. The sorption behaviour of MB onto OPEFB char was analysed using non-linear regression and

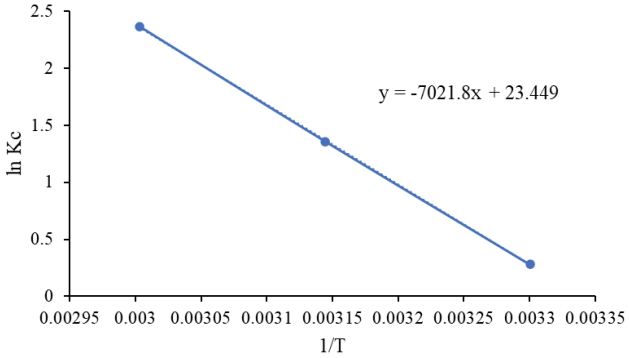

Fig. 6. Graph of thermodynamic study.

Table 2
Thermodynamic parameters for adsorption of MB on treated OPEFB char

$\Delta H°$ (kJ/mol)	$\Delta S°$ (J/mol·K)	$-\Delta G°$ (kJ/mol)		
		303 K	318 K	333 K
58.379	194.955	0.70505	3.5925	6.5562

the results are summarized in Table 3. The fitness of the model is evaluated based on the value of the correlation coefficient, R^2. Table 3 shows the values of maximum adsorption amount (Q_{max}), correlation coefficient (R^2) and other parameters calculated from the data fitted by the isotherms at temperature 30°C.

From Table 3, the Langmuir isotherm model generates a correlation factor, R^2 of 0.8682 which shows it does not fit well into the model. It has been observed that the maximum adsorption capacity (Q_{max}) was found to be 167.2 mg/g. It can be seen that Freundlich isotherm model fitted well with the experimental data better than Langmuir isotherm model with highest R^2 (0.9352), suggesting the non-ideal, reversible and multilayer adsorption over the heterogeneous surface. The Freundlich model's $1/n$ value is 0.1232, or n value is 8.114, which is greater than one, indicating that MB adsorption on this treated OPEFB char is favorable. Therefore, it can be concluded that MB adsorption onto treated OPEFB char involves a multilayer adsorption and a heterogeneous surfaces with non-uniform distribution of adsorption heat [56].

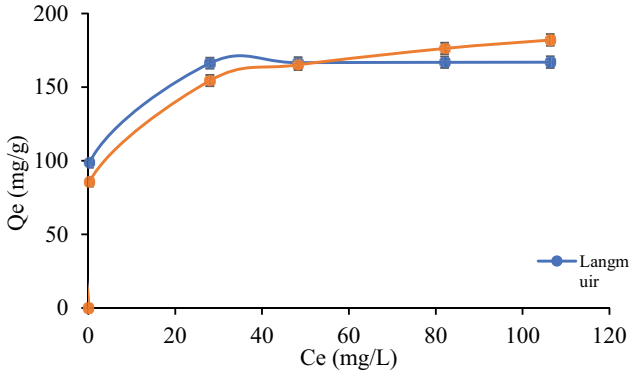

Fig. 7. Model fit of adsorption isotherm of MB adsorption onto treated OPEFB char at 30°C.

3.7. Kinetic studies

In this study, the mechanism of the adsorption of MB onto treated OPEFB char was investigated using pseudo-first-order and pseudo-second-order kinetics. Table 4 presents the kinetic constants obtained by fitting the kinetic data using non-linear regression analysis and their corresponding non-linear curves are shown in Figs. 8 and 9. The data on Q_t vs. time in Fig. 8 were plotted to obtain the values of k_1. The correlation factors (R^2) are from the range of 0.8877 to 0.9740 for different concentrations of MB (100, 150, 200, 250 and 300 ppm). These values are not agreeable to the experimental results and therefore do not follow the first order kinetics of pseudo-first-order model.

k_2 is the rate constant of the pseudo-second-order kinetics model, whose values can be obtained by plotting Q_t vs. time in Fig. 9. The values for correlation coefficients R^2 for pseudo-second-order kinetics model are in the range of 0.9216–0.9581 which shows that the kinetic chosen is at good agreement with the experimental data. The values of calculated, $Q_{e(calc)}$ in Table 4 are comparable with the experimental data, $Q_{e(exp)}$ for pseudo-second-order kinetic model compared to the pseudo-first-order kinetic model. The predicted equilibrium adsorption capacity fit the actual equilibrium adsorption capacity very well. This agrees with the R^2 values obtained and proves that the adsorption of MB onto the treated OPEFB char could be best fitted described by the pseudo-second-order kinetic model which is based

Table 3
Isotherm parameters and correlation coefficients for MB adsorption onto treated OPEFB char at 30°C

Langmuir			Freundlich		
Q_{max} (mg/g)	K_L (L/mg)	R^2	K_f (mg/g·(L/mg)$^{1/n}$)	n	R^2
167.2	6.145	0.8682	102.4	8.114	0.9352

Table 4
Kinetic parameters and correlation coefficients for MB adsorption onto treated OPEFB char at 30°C

Pseudo-first-order				
Concentration mg/L	$Q_{e(exp)}$ (mg/g)	$Q_{e(calc)}$ (mg/g)	k_1 (h)	R^2
100	99.419	96.14	0.3004	0.8877
150	127.017	124.3	0.3028	0.9375
200	149.644	151.1	0.2628	0.9612
250	186.239	198.6	0.1913	0.9839
300	203.290	223.5	0.1580	0.9740
Pseudo-second-order				
Concentration mg/L	$Q_{e(exp)}$ (mg/g)	$Q_{e(calc)}$ (mg/g)	k_2 (h)	R^2
100	99.419	107.9	0.004002	0.9216
150	127.017	142.6	0.002775	0.9560
200	149.644	178.0	0.001747	0.9624
250	186.239	251.8	0.0007236	0.9686
300	203.290	294.7	0.0004675	0.9581

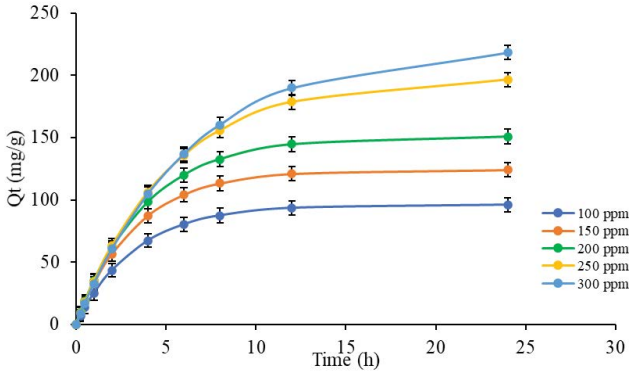

Fig. 8. Pseudo-first-order kinetics for adsorption of MB adsorption onto treated OPEFB char.

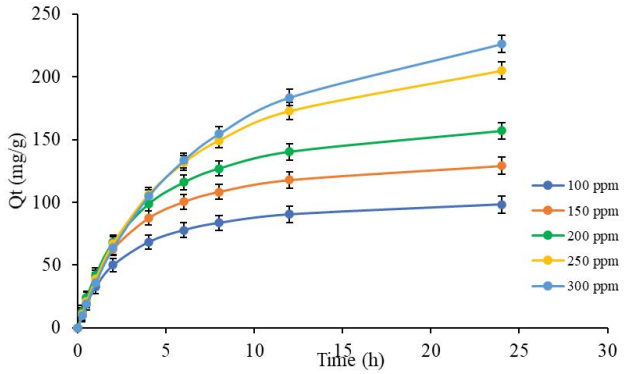

Fig. 9. Pseudo-second-order kinetics for adsorption of MB adsorption onto treated OPEFB char.

on the equilibrium chemical adsorption, that predicts the behaviour over the whole range of studies, strongly supporting the validity and agrees with chemisorption being rate-controlling [57].

3.8. Comparison with other adsorbents

The values of the MB adsorption capacities from different source of low-cost adsorbents are summarized in Table 5. From the comparison, OPEFB char can be considered as a valuable and competitive adsorbent for the removal of MB from aqueous solution owing to its high adsorption capacity value.

4. Conclusion

This study showed that the treated OPEFB char possessed excellent characteristic for MB adsorption. The OPEFB char was utilized as a feedstock for preparation of AC through H_3PO_4 chemical activation. The FTIR analysis demonstrated the existance of O–H, C=C and C=O groups. The images from SEM showed that the porous structure of OPEFB char improved significantly after H_3PO_4 treatment which was supported by the increment of BET surface area from 258.87 to 345.43 m^2/g. The effect of contact time, pH and temperature on the MB adsorption were studied. The highest MB adsorption was found at pH, 6; temperature, 60°C and contact time 24 h with 91.44% of MB removal. The kinetic and isotherm data fitted well with pseudo-second-order kinetic and Freundlich isotherm models. The negative value of $\Delta G°$ and positive values of $\Delta H°$ indicated that the adsorption process was an endothermic and spontaneous process. These results proved that the treated OPEFB char could be employed as adsorbent as an alternative to the commercial AC for the removal of cationic dyes from industrial wastewater.

Table 5
Comparison of MB adsorption capacities from various adsorbents

Adsorbent	Adsorption capacity (mg/g)	References
Eucalyptus leaves	52.2	[58]
Spent tea residue	93.5	[59]
Coriandrum sativum	94.9	[60]
Pterospermum acerifolium shells	250.0	[61]
Sterculia foetida	181.8	[62]
Agave salmiana leaves	188.7	[63]
Garcinia mangostana	163.6	[52]
Corn stalk	149.0	[64]
OPEFB char	167.2	This study

Acknowledgements

The author would like to thank Universiti Malaysia Perlis and Centre of Excellence, Water Research and Environmental Sustainability Growth (WAREG) for the facilities and funds provided to conduct this research.

References

[1] D. Badis, Z. Benmaamar, O. Benkortbi, H. Boutoumi, H. Hamitouche, A. Aggoun, Removal of methylene blue by adsorption onto retama raetam plant: kinetics and equilibrium study, Chem. J. MOLDOVA, 11 (2016) 74–83.
[2] R. Farma, F. Wahyuni, Awitdrus, Physical properties analysis of activated carbon from oil palm empty fruit bunch fiber on methylene blue adsorption, J. Technomaterial Phys., 1 (2019) 67–73.
[3] R. Abu-El-Halawa, S.A. Zabin, H.H. Abu-Sittah, Investigation of methylene blue dye adsorption from polluted water using oleander plant (Al defla) tissues as sorbent, Am. J. Environ. Sci., 12 (2016) 213–224.
[4] C.M. Chan, S.X. Chin, S.W. Chook, C.H. Chia, S. Zakaria, Combined mechanical-chemical pre-treatment of oil palm empty fruit bunch (EFB) fibers for adsorption of methylene blue (MB) in aqueous solution, Malays. J. Anal. Sci., 22 (2018) 1007–1013.
[5] Y. Kuang, X. Zhang, S. Zhou, Adsorption of methylene blue in water onto activated carbon by surfactant modification, Water (Switzerland), 12 (2020) 1–19.
[6] A. Azari, M. Yeganeh, M. Gholami, M. Salari, The superior adsorption capacity of 2,4-Dinitrophenol under ultrasound-assisted magnetic adsorption system: modeling and process optimization by central composite design, J. Hazard. Mater., 418 (2021) 126348, doi: 10.1016/j.jhazmat.2021.126348.

[7] Y. Rashtbari, S. Hazrati, A. Azari, S. Afshin, M. Fazlzadeh, M. Vosoughi, A novel, eco-friendly and green synthesis of PPAC-ZnO and PPAC-nZVI nanocomposite using pomegranate peel: cephalexin adsorption experiments, mechanisms, isotherms and kinetics, Adv. Powder Technol., 31 (2020) 1612–1623.
[8] A. Azari, R. Nabizadeh, A.H. Mahvi, S. Nasseri, Integrated fuzzy AHP-TOPSIS for selecting the best color removal process using carbon-based adsorbent materials: multi-criteria decision making vs. systematic review approaches and modeling of textile wastewater treatment in real conditions, Int. J. Environ. Anal. Chem., 102 (2020) 7329–7344.
[9] D.L. Postai, C.A. Demarchi, F. Zanatta, D.C.C. Melo, C.A. Rodrigues, Adsorption of rhodamine B and methylene blue dyes using waste of seeds of Aleurites Moluccana, a low cost adsorbent, Alexandria Eng. J., 55 (2016) 1713–1723.
[10] D. Lan, H. Zhu, J. Zhang, S. Li, Q. Chen, C. Wang, T. Wu, M. Xu, Adsorptive removal of organic dyes via porous materials for wastewater treatment in recent decades: a review on species, mechanisms and perspectives, Chemosphere, 293 (2022) 133464, doi: 10.1016/j.chemosphere.2021.133464.
[11] G. Ravenni, G. Cafaggi, Z. Sárossy, K.T. Rohde Nielsen, J. Ahrenfeldt, U.B. Henriksen, Waste chars from wood gasification and wastewater sludge pyrolysis compared to commercial activated carbon for the removal of cationic and anionic dyes from aqueous solution, Bioresour. Technol. Rep., 10 (2020) 100421, doi: 10.1016/j.biteb.2020.100421.
[12] A.A. Ahmad, A.T.M. Din, N.K.E. Yahaya, A. Khasri, M.A. Ahmad, Adsorption of basic green 4 onto gasified *Glyricidia sepium* woodchip based activated carbon: optimization, characterization, batch and column study, Arabian J. Chem., 13 (2020) 6887–6903.
[13] H. Jung, D.D. Sewu, G. Ohemeng-Boahen, D.S. Lee, S.H. Woo, Characterization and adsorption performance evaluation of waste char by-product from industrial gasification of solid refuse fuel from municipal solid waste, Waste Manage., 91 (2019) 33–41.
[14] R.M. Raj, M. Asaithambi, Microwave assisted chemical activation of papaya leaf stem activated carbon for the removal of dyes from aqueous solution, J. Environ. Nanotechnol., 3 (2014) 91–95.
[15] V. Benedetti, F. Patuzzi, M. Baratieri, Characterization of char from biomass gasification and its similarities with activated carbon in adsorption applications, Appl. Energy, 227 (2018) 92–99.
[16] A.A. Ahmad, N.A. Zawawi, F.H. Kasim, A. Inayat, A. Khasri, Assessing the gasification performance of biomass: a review on biomass gasification process conditions, optimization and economic evaluation, Renewable Sustainable Energy Rev., 53 (2016) 1333–1347.
[17] G. Itskos, N. Margaritis, A. Koutsianos, P. Grammelis, Characterization of solid residues from high temperature gasification of olive kernel, Waste Biomass Valorization, 5 (2014) 893–901.
[18] X. Tang, N. Ripepi, High pressure supercritical carbon dioxide adsorption in coal: adsorption model and thermodynamic characteristics, J. CO_2 Util., 18 (2017) 189–197.
[19] T. Xu, Y. Wu, S. Bhattacharya, Gasification kinetic modelling of victorian brown coal chars and validity for entrained flow gasification in CO_2, Int. J. Min. Sci. Technol., 31 (2021) 473–481.
[20] R. Wei, L. Ren, F. Geng, Gasification reactivity and characteristics of coal chars and petcokes, J. Energy Inst., 96 (2021) 25–30.
[21] M. Sajid, A. Raheem, N. Ullah, M. Asim, M.S. Ur Rehman, N. Ali, Gasification of municipal solid waste: progress, challenges, and prospects, Renewable Sustainable Energy Rev., 168 (2022) 112815, doi: 10.1016/j.rser.2022.112815.
[22] A.R. Saleh, B. Sudarmanta, H. Fansuri, O. Muraza, Syngas production from municipal solid waste with a reduced tar yield by three-stages of air inlet to a downdraft gasifier, Fuel, 263 (2020) 116509, doi: 10.1016/j.fuel.2019.116509.
[23] P. Mondal, From municipal solid waste (MSW) to hydrogen: performance optimization of a fixed bed gasifier using Box–Benkhen method, Int. J. Hydrogen Energy, 47 (2022) 20064–20075.
[24] S. Banerjee, G.C. Sharma, R.K. Gautam, M.C. Chattopadhyaya, S.N. Upadhyay, Y.C. Sharma, Removal of malachite green, a hazardous dye from aqueous solutions using avena sativa (oat) hull as a potential adsorbent, J. Mol. Liq., 213 (2016) 162–172.
[25] T. Maneerung, J. Liew, Y. Dai, S. Kawi, C. Chong, C.H. Wang, Activated carbon derived from carbon residue from biomass gasification and its application for dye adsorption: kinetics, isotherms and thermodynamic studies, Bioresour. Technol., 200 (2016) 350–359.
[26] W.M.S. Wan Ismail, R.A. Rasid, Empty fruit bunch (EFB) gasification in an entrained flow gasification system, Chem. Eng. Res. Bull., 19 (2017) 43–49.
[27] G. Su, N.W. Mohd Zulkifli, H.C. Ong, S. Ibrahim, Q. Bu, R. Zhu, Pyrolysis of oil palm wastes for bioenergy in Malaysia: a review, Renewable Sustainable Energy Rev., 164 (2022) 112554, doi: 10.1016/j.rser.2022.112554.
[28] A.A. Ahmad, A.T.M. Din, N.K.E.M. Yahaya, J. Karim, M.A. Ahmad, Atenolol sequestration using activated carbon derived from gasified *Glyricidia sepium*, Arabian J. Chem., 13 (2020) 7544–7557.
[29] N. Intarachandra, S. Siriworakon, T. Sangmanee, Preparation of oil palm empty fruit bunch based activated carbon for adsorption of dye from aqueous solution, MATEC Web Conf., 268 (2019) 06008, doi: 10.1051/matecconf/201926806008.
[30] A. Khasri, M.R.M. Jamir, A.A. Ahmad, M.A. Ahmad, Adsorption of remazol brilliant violet 5r dye from aqueous solution onto melunak and rubberwood sawdust based activated carbon: interaction mechanism, isotherm, kinetic and thermodynamic properties, Desal. Water Treat., 216 (2021) 401–411.
[31] M.A. Islam, M.J. Ahmed, W.A. Khanday, M. Asif, B.H. Hameed, Mesoporous activated carbon prepared from NaOH activation of rattan (*Lacosperma secundiflorum*) hydrochar for methylene blue removal, Ecotoxicol. Environ. Saf., 138 (2017) 279–285.
[32] M.F.M. Yusop, M.A. Ahmad, N.A. Rosli, M.E.A. Manaf, Adsorption of cationic methylene blue dye using microwave-assisted activated carbon derived from acacia wood: optimization and batch studies, Arabian J. Chem., 14 (2021) 103122, doi: 10.1016/j.arabjc.2021.103122.
[33] C. Ooi, T. Lee, S. Pung, F. Yeoh, Activated carbon fiber derived from single step carbonization-activation process, ASEAN Eng. J., 4 (2015) 40–50.
[34] A.A. Adeyi, S.N.A.M. Jamil, L.C. Abdullah, T.S.Y. Choong, Adsorption of malachite green dye from liquid phase using hydrophilic thiourea-modified poly(acrylonitrile-*co*-acrylic acid): kinetic and isotherm studies, J. Chem., 2019 (2019) 4321475 (1–14), doi: 10.1155/2019/4321475.
[35] N.B. Osman, N. Shamsuddin, Y. Uemura, Activated carbon of oil palm empty fruit bunch (EFB); core and shaggy, Procedia Eng., 148 (2016) 758–764.
[36] A.A. Ahmad, M.A. Ahmad, N.K.E.M. Yahaya, J. Karim, Adsorption of malachite green by activated carbon derived from gasified *Hevea brasiliensis* root, Arabian J. Chem., 14 (2021) 103104, doi: 10.1016/j.arabjc.2021.103104.
[37] A. Khasri, O.S. Bello, M.A. Ahmad, Mesoporous activated carbon from pentace species sawdust via microwave-induced KOH activation: optimization and methylene blue adsorption, Res. Chem. Intermed., 44 (2018) 1–21.
[38] R. Wirasnita, T. Hadibarata, A.R.M. Yusoff, Z. Mat Lazim, Preparation and characterization of activated carbon from oil palm empty fruit bunch wastes using zinc chloride, J. Teknol., 74 (2015) 77–81.
[39] Y. Sudaryanto, S.B. Hartono, W. Irawaty, H. Hindarso, S. Ismadji, High surface area activated carbon prepared from cassava peel by chemical activation, Bioresour. Technol., 97 (2006) 734–739.
[40] F.A. Daud, N. Ismail, R.M. Ghazi, Response surface methodology optimization of methylene blue removal by activated carbon derived from foxtail palm tree empty fruit bunch, J. Trop. Resour. Sustain. Sci., 4 (2016) 25–30.
[41] P.K. Singh, S. Banerjee, A.L. Srivastava, Y.C. Sharma, Kinetic and equilibrium modeling for removal of nitrate from aqueous solutions and drinking water by a potential adsorbent, hydrous bismuth oxide, RSC Adv., 5 (2015) 35365–35376.

[42] N. Ahmad, N. Ibrahim, P.Y. Fu, R. Ahmad, Influence of carbonisation temperature on the surface pore characteristics of acid-treated oil palm empty fruit bunch activated carbon, J. Teknol., 82 (2020) 127–133.
[43] A. Khasri, A.A. Ahmad, M.A. Ahmad, Preparation of activated carbon by microwave-induced KOH activation and its application in dye removal, AIP Conf. Proc., 2124 (2019) 020054, doi: 10.1063/1.5117114.
[44] K.Y. Foo, B.H. Hameed, Adsorption characteristics of industrial solid waste derived activated carbon prepared by microwave heating for methylene blue, Fuel Process. Technol., 99 (2012) 103–109.
[45] M.M. Almoneef, J. Rouabeh, M. Mbarek, Theoretical assessment of the adsorption mechanism of methylene blue and malachite green on metalloporphyrin, Synth. Met., 290 (2022) 117158, doi: 10.1016/j.synthmet.2022.117158.
[46] C. Djilani, R. Zaghdoudi, F. Djazi, B. Bouchekima, A. Lallam, A. Modarressi, M. Rogalski, Adsorption of dyes on activated carbon prepared from apricot stones and commercial activated carbon, J. Taiwan Inst. Chem. Eng., 53 (2015) 112–121.
[47] S. Zhou, Z. Du, X. Li, Y. Zhang, Y. He, Y. Zhang, Degradation of methylene blue by natural manganese oxides: kinetics and transformation products, R. Soc. Open Sci., 6 (2019) 190351, doi: 10.1098/rsos.190351.
[48] L. Yu, Y. Luo, Journal of environmental chemical engineering the adsorption mechanism of anionic and cationic dyes by Jerusalem artichoke stalk-based mesoporous activated carbon, Biochem. Pharmacol., 2 (2014) 220–229.
[49] M.S. Sajab, C.H. Chia, S. Zakaria, P.S. Khiew, Cationic and anionic modifications of oil palm empty fruit bunch fibers for the removal of dyes from aqueous solutions, Bioresour. Technol., 128 (2013) 571–577.
[50] S. Soleimani, A. Heydari, M. Fattahi, A. Motamedisade, Calcium alginate hydrogels reinforced with cellulose nanocrystals for methylene blue adsorption: synthesis, characterization, and modelling, Ind. Crops Prod., 192 (2023) 115999, doi: 10.1016/j.indcrop.2022.115999.
[51] L. Mouni, L. Belkhiri, J.C. Bollinger, A. Bouzaza, A. Assadi, A. Tirri, F. Dahmoune, K. Madani, H. Remini, Removal of methylene blue from aqueous solutions by adsorption on kaolin: kinetic and equilibrium studies, Appl. Clay Sci., 153 (2018) 38–45.
[52] A.H. Jawad, S.E.M. Saber, A.S. Abdulhameed, A. Reghioua, Z.A. ALOthman, L.D. Wilson, Mesoporous activated carbon from mangosteen (*Garcinia mangostana*) peels by H_3PO_4 assisted microwave: optimization, characterization, and adsorption mechanism for methylene blue dye removal, Diamond Relat. Mater., 129 (2022) 109389, doi: 10.1016/j.diamond.2022.109389.
[53] Y. Wang, C. Srinivasakannan, H. Wang, G. Xue, L. Wang, X. Wang, X. Duan, Preparation of novel biochar containing graphene from waste bamboo with high methylene blue adsorption capacity, Diamond Relat. Mater., 125 (2022) 109034, doi: 10.1016/j.diamond.2022.109034.
[54] L.F.B. de Araújo, S.E. Mazzetto, D. Lomonaco, F. Avelino, Unraveling the adsorption mechanism of methylene blue onto selective pH precipitated kraft lignins: kinetic, equilibrium and thermodynamic aspects, Int. J. Biol. Macromol., 220 (2022) 1267–1276.
[55] O. Amrhar, H. Nassali, M. Elyoubi, Application of nonlinear regression analysis to select the optimum absorption isotherm for methylene blue adsorption onto natural illitic clay, Bull. La Société R. Des Sci. Liège, 84 (2015) 116–130.
[56] S. Gholitabar, H. Tahermansouri, Kinetic and multi-parameter isotherm studies of picric acid removal from aqueous solutions by carboxylated multi-walled carbon nanotubes in the presence and absence of ultrasound, Carbon Lett., 22 (2017) 14–24.
[57] F. Ullah, G. Ji, M. Irfan, Y. Gao, F. Shafiq, Y. Sun, Q.U. Ain, A. Li, Adsorption performance and mechanism of cationic and anionic dyes by KOH activated biochar derived from medical waste pyrolysis, Environ. Pollut., 314 (2022) 120271, doi: 10.1016/j.envpol.2022.120271.
[58] K. Ghosh, N. Bar, A. Baran Biswas, S.K. Das, Removal of methylene blue by H_3PO_4 treated eucalyptus leaves: study of fixed bed column and GA-ANN modeling, Sustainable Chem. Pharm., 29 (2022) 100774, doi: 10.1016/j.scp.2022.100774.
[59] E. Salehi, M. Askari, M. Velashjerdi, B. Arab, Phosphoric acid-treated spent tea residue biochar for wastewater decoloring: batch adsorption study and process intensification using multivariate data-based optimization, Chem. Eng. Process. Process Intensif., 158 (2020) 108170, doi: 10.1016/j.cep.2020.108170.
[60] C.C. de Souza, L.Z.M. de Souza, M. Yılmaz, M.A. de Oliveira, A.C. da Silva Bezerra, E.F. da Silva, M.R. Dumont, A.R.T. Machado, Activated carbon of *Coriandrum sativum* for adsorption of methylene blue: equilibrium and kinetic modeling, Cleaner Mater., 3 (2022) 100052, doi: 10.1016/j.clema.2022.100052.
[61] S. Rangabhashiyam, P. Balasubramanian, Adsorption behaviors of hazardous methylene blue and hexavalent chromium on novel materials derived from *Pterospermum acerifolium* shells, J. Mol. Liq., 254 (2018) 433–445.
[62] S. Basu, G. Ghosh, S. Saha, Adsorption characteristics of phosphoric acid induced activation of bio-carbon: equilibrium, kinetics, thermodynamics and batch adsorber design, Process Saf. Environ. Prot., 117 (2018) 125–142.
[63] R.A. Canales-Flores, F. Prieto-García, Taguchi optimization for production of activated carbon from phosphoric acid impregnated agricultural waste by microwave heating for the removal of methylene blue, Diamond Relat. Mater., 109 (2020) 108027, doi: 10.1016/j.diamond.2020.108027.
[64] Y. Tang, Y. Zhao, T. Lin, Y. Li, R. Zhou, Y. Peng, Adsorption performance and mechanism of methylene blue by H_3PO_4-modified corn stalks, J. Environ. Chem. Eng., 7 (2019) 103398, doi: 10.1016/j.jece.2019.103398.